Indian Journal of Chemistry
Vol. 62, August 2023, pp. 834-842
DOI: 10.56042/ijc.v62i8.4767

Basic Red 9 dye encapsulated graphene oxide-montmorillonite composite: Fluorescent and electrochemical sensor for dopamine in presence of ascorbic acid and uric acid

Sarojmoni Kalita & Diganta Kumar Das*
Department of Chemistry, Gauhati University, Guwahati 781 014, Assam, India
E-mail: diganta_chem@gauhati.ac.in

Received 3 June 2022; accepted (revised) 13 July 2023

The dye Basic Red 9 has been successfully encapsulated into GO-MMT composite and the probe acts as a "turn on" fluorescence sensor for dopamine (DA) in presence of its main biological counterpart *i.e.* ascorbic acid (AA), uric acid (UA) along with other biologically important ions and molecules. The limit of detection (LOD) for dopamine detection is found to be 6.57 nM and 5.05 nM in the absence and presence of AA and UA respectively. Glassy carbon electrode modified with the sensor can successfully distinguish between the peaks of DA, AA and UA by cyclic voltammetry technique. The LOD for AA, UA and DA have been calculated as 1.165 nM, 0.875 nM and 3.043 nM respectively. The voltammetric detection of mixture containing DA, AA and UA are free from common interfering ions and species like glucose, cholesterol, Na^+, K^+ , Ca^{2+}, Fe^{2+}.

Keywords: Basic Red 9, Dopamine, Ascorbic acid, Uric Acid, Fluorescence, Voltammetry

3,4-Dihydroxyphenyl ethylamine or dopamine (DA) belonging to the catecholamine family of neurotransmitters, playing important role in human metabolism, renal system, peripheral nervous system, hormonal system, as well as the central nervous system and the cardiovascular system has been widely studied over the last few years for its impact upon human behavioral responses including mood, anxiety, addiction and memory[1-4]. Moreover, DA acts upon the sympathetic nervous system, to produce effects such as increased heart rate and blood pressure[5]. Huntington's disease may be caused by high DA concentration levels in the blood[6] whereas low DA level causes neurological disorders such as Parkinson's disease, schizophrenia, ADHD, autism, fibromyalgia, Alzheimer's disease, *etc*.[7,8] Hence detection of DA is essential for controlling hormonal balance as well as diagnosing and preventing the diseases mentioned. Several techniques such as flow-injection analysis[9], chemiluminescence[10], electrochemistry[11], capillary electrophoresis[12], UV–Vis spectroscopy[13], fluorescence spectroscopy[14], liquid chromatography[15], mass spectrometry chromatography[16], *etc*. have been developed for detection of DA. The primary issue in the detection and accurate measurement of DA in biological samples is due to its co-existence with uric acid (UA) and ascorbic acid (AA) in extracellular fluid, serum, and central nervous system[17] and overlapped voltammetric response (reversible oxidation of DA and irreversible oxidation of AA and UA) due to similar oxidation potential at conventional solid electrodes[18]. Due to the electro-active nature of DA, AA, and UA, fluorescent and electrochemical sensors are being significantly used for simultaneous detection of the above- mentioned molecules as other analytical techniques involve expensive instrumentation, time-consuming analysis[19] while fluorescence spectroscopy and electrochemical methods involve simple environmental friendly detection, and provide convenient, reproducible, rapid, precise, highly sensitive and selective results[20].

Carbon-based materials such as fullerene C_{60}, nanotubes, carbon black/carbon nanopowder, graphene, *etc*. have been extensively explored on the account of being environmentally and biologically friendly[21]. In particular, due to excellent mechanical, thermal, and electrical properties, graphene or graphene oxide (GO) has been intensively studied in material science[22]. Owing to its 2D honeycomb-like structure and high surface area as well as superior electrical property,

adsorption capacity and strong hydrophilic nature, GO has been proposed as a novel substitute for graphene[23-25]. However, one of the major drawbacks of exploiting GO is that it aggregates irreversibly leading to a loss in adsorption capacity and recyclability of materials[26]. To overcome this problem, researchers have been using graphene oxide-clay composite in various applications[27]. Montmorillonite clay (MMT) belonging to the smectite clay group is the commonly used layered silicate due to its vast cation exchange capability, high porosity, peculiar layered structure, non toxicity and abundant occurrence in most soil types[28,29]. These nanohybrids exhibit enhanced gas permeability, thermal stability, and flame retardancy and proved to be helpful in the development of electrochemical sensors and biosensors for a wide range of biomolecules, chemicals and gases[30,31]. Tandel *et al*. synthesized bentonite-reduced graphene oxide composite as a sensor for the neurotransmitter dopamine[32]. In a recent study, Ding *et al*. prepared graphene oxide/clay composite for simultaneous detection of AA, UA and DA[33]. In another report, Li *et al*. developed a clay-graphene hybrid for the facile detection of dopamine[34].

Due to their excellent sensitivity to the environment and electrocatalytic properties, dyes have been efficiently used as optical sensors and chemosensors for chemical/biological molecules[35]. They can be easily assembled onto the surface of nanomaterials to form functional nanocomposites[36]. Kalita *et al*. reported rosaniline hydrochloride encapsulated MCM-48 as a fluorescent and electrochemical sensor for DA and AA[20]. Su *et al*. has developed molybdenum disulfide@Methylene Blue nanohybrid for electrochemical determination of microRNA-21, UA and DA[37].

In this paper, we report that Basic Red 9 dye encapsulated in GO-MMT composite (BR9@GO-MMT) acts as a fluorescent sensor for the neurotransmitter dopamine (DA) in presence of its chief coexisting biomolecules and metal ions in biological medium. Glassy carbon electrode modified with BR9@GO-MMT nanocomposite leads to a significant difference in oxidation potential of DA, AA and UA in their mixture. The sensor has also been successfully applied for dopamine detection in bovine serum albumin. The limits of detection of DA in presence of interfering ions are also reported.

Experimental Section

Materials

Montmorillonite K10 clay, Basic Red 9 dye (BR9), Potassium permanganate ($KMnO_4$), sodium nitrate ($NaNO_3$), concentrated sulphuric acid (H_2SO_4, 98% (w/w)), hydrochloric acid (HCl), hydrogen peroxide (H_2O_2, 30% (w/w)), Dopamine (DA), Ascorbic acid (AA), Uric acid (UA), other biomolecules and all other chemicals were purchased either from Sigma Aldrich or LOBA. The chemicals were of analytical grade and used without further purification. The chemical solutions were prepared in de-ionized water obtained from quartz double distilled plant. The graphite rods were extracted from used dry cells (Eveready Battery 1.5 V). The FT-IR spectra were recorded in a Perkin Elmer RXI spectrometer as KBr pellets. The fluorescence and UV-Visible spectra were recorded in HITACHI 2500 and Shimadzu UV 1800 spectrophotometer respectively using quartz cuvette (1cm path length). The electrochemical measurements were carried out on a CHI660DCH Instrument electrochemical analyser (USA) consisting of a three-electrode system: Glassy carbon (GC) electrode as the working electrode, Ag/AgCl (3M NaCl) as the auxiliary electrode, Pt wire as the reference electrode and 1M KCl as supporting electrolyte. Scanning Electron Microscopy was done using Zeiss FESEM Sigma 300 and Energy Dispersive X-ray Spectroscopy was studied using Ametek EDAX. Powder X-ray diffraction (PXRD) patterns of the synthesized samples were recorded using a Rigaku Ultima IV X-Ray diffractometer (Cu K_α radiation, λ=1.5418 Å) at 40 kV and 40 mA. Thermogravimetric analysis (TGA) was done using Metter Toledo TGA/DSC1 STAR^e system in presence of N_2 atmosphere in the temperature range 50-700 °C at a heating rate of 10 °C/min.

Synthesis of Graphene Oxide (GO)

Graphene Oxide was prepared from graphite rods (extracted from used dry cells) using a modified Hummer's method. 0.5 g of graphite rod and 0.5 g $NaNO_3$ were added to 24 mL concentrated H_2SO_4. The mixture was kept in an ice bath keeping the temperature at approximately 5°C and ultrasonicated for 1 h. Then 3 g of $KMnO_4$ was gradually added keeping the temperature of the mixture below 15°C. The mixture was stirred by ultrasonication for 2 h to get a homogeneous mixture. 100 mL deionized water was slowly added to the mixture followed by

ultrasonication for 1 h producing a brown-colored mixture. The mixture was removed from the ice bath and stirred magnetically for 1 h and the temperature was increased to 35°C when the color of the mixture changed to light brown. Afterward another 100 mL of deionized water was added to the mixture and the temperature was increased to 90°C and stirred for 1 h. In the end, a solution of 10 mL H_2O_2 and 100 mL deionized water was added to obtain a light-yellow suspension. The suspension so obtained was filtered with high-quality Wattman filter and washed with 10% HCl to remove metal ions and at last washed with deionized water till *p*H becomes neutral. The filtrate was then mixed with deionized water and ultrasonicated for 1 h to obtain a dispersion of Graphene Oxide (GO) solution. The dispersion was then centrifuged at 5000 rpm for 30 min to remove non-exfoliated graphite and other impurities. This solution was then filtered and dried. Finally, a brown-colored graphene oxide (GO) powder was obtained (Scheme 1).

Synthesis of montmorillonite-graphene oxide com posite

Firstly, the montmorillonite clay was acid treated by refluxing 10g of it in 200 mL of 2M HCl solution for 2 h. The above clay powder was then filtered and rinsed repeatedly with distilled water until no Cl^- ions could be detected by the $AgNO_3$ test. The activated clay was oven-dried at 60 °C for 12 h. For the preparation of the composite, 2.5 g of GO was mixed with 5 g of the modified montmorillonite clay in 30 mL deionised water and sonicated for 2 h and stirred for 1 h. Finally, the mixture was filtered and dried in an oven for 24 h. The light grey colored composite was named GO-MMT composite (Scheme 2).

Synthesis of the Sensor (BR9@GO-MMT)

2 g of GO-MMT composite was suspended in 20 mL double distilled water and stirred for 15 min. To the suspension, 0.5 g of the BR9 dye was added with continuous stirring for 36 h. The dye loaded GO-MMT composite was centrifuged, and washed with deionsed water. The dark maroon solid was oven dried at 120 °C for 18 h to finally obtain the BR9@GO-MMT composite (Scheme 3).

Preparation of Modified GC electrode (BR9@GO-MMT/GC)

The electrode was pre-cleaned before modification as per reported[38]. The electrode modification was

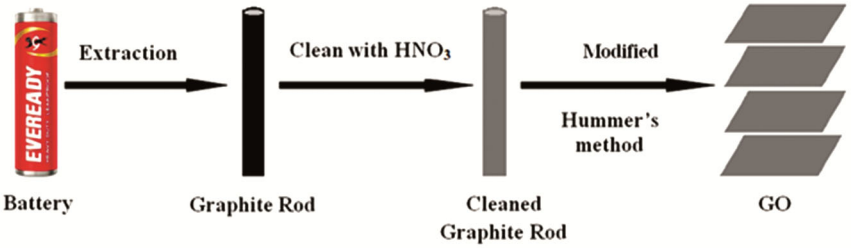

Scheme 1 — Preparation of Graphene Oxide (GO)

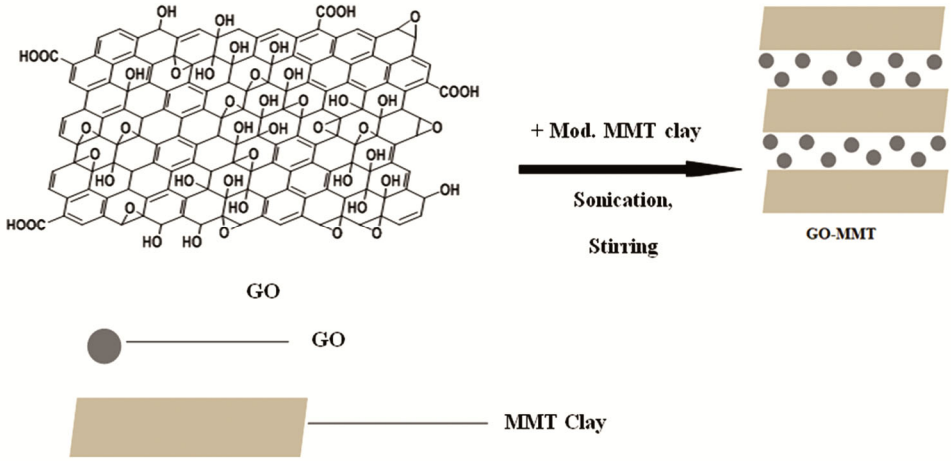

Scheme 2 — Synthesis of GO-MMT composite

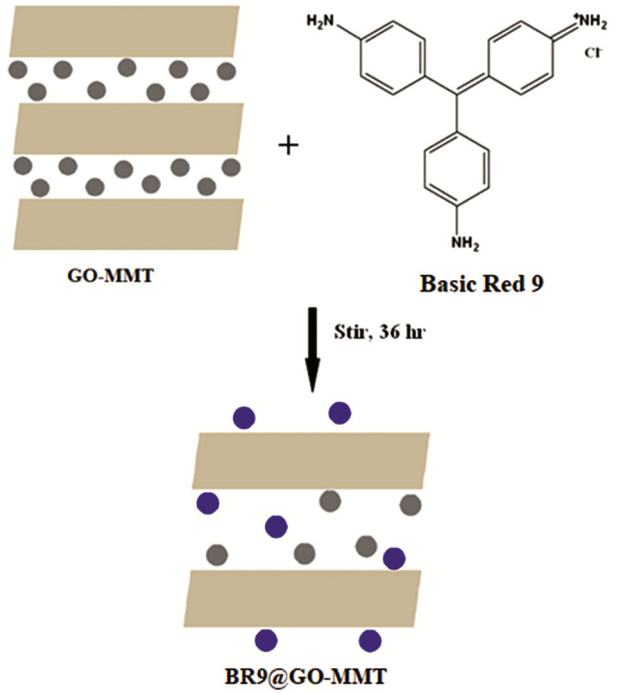

Scheme 3 — Synthesis of BR9@GO-MMT

done as follows: 10mg of the sensor BR9@GO-MMT was dispersed in 1 mL of acetonitrile and 0.5 mL of styrene. 1µL of the solution was placed on the tip of a glassy carbon electrode with the help of a micropipette. The process was repeated three times and the modified electrodes were allowed to dry.

Results and Discussion

Characterization of the materials

The FTIR spectra of GO, MMT, GO-MMT and BR9@GO-MMT are shown in figure S1a and S1b. In the case of GO, the band at 3450 cm^{-1} is due to OH stretching mode, bands centered around 1730 cm^{-1}, 1650 cm^{-1}, 1400 cm^{-1}, and 1050 cm^{-1} indicate the presence of C=O, aromatic C=C, hydroxyl C-OH, and epoxy C-O-C vibrations respectively. In the FTIR spectra of MMT clay, a broad transmittance band can be seen in the 3800-3000 cm^{-1} region, with peak maxima at 3620 cm^{-1} and 3400 cm^{-1} corresponding to octahedral Al-OH group and the O-H stretching vibrational modes of water. The bands at 1640 cm^{-1} and 1200-1000 cm^{-1} range are due to O-H bending vibration and Si-O, Al-O-Si stretching and anti-symmetric vibrations respectively. The bending vibrational modes of O-Si-O and Si-O-Al are observed at 820 cm^{-1} and 530 cm^{-1} respectively. All the characteristic bands are retained in the GO-clay composite, with minor shifts and decrease in peak intensity observed. The intensity of the peak at 1400 cm^{-1} corresponding to the C-OH group increases which is an indication of partial reduction of GO in the GO-MMT composite. In the dye encapsulated GO-MMT composite, a series of bands appear in the region 1600-1350 cm^{-1} in the spectra which are due to the presence of the host molecule in the nanocomposite. The peak at 1590 cm^{-1} is due to the NH_2 group of the dye respectively.

The powder XRD pattern of GO, MMT, GO-MMT and dye encapsulated GO-MMT is depicted in figure S2. The XRD pattern of GO shows a characteristic diffraction peak at 10.5° corresponding to (001) plane. In case of MMT clay, the reflections occur at 8.85°, 22°, 35°, 55°, and 62° which correspond to (110), (105), (210) and (300) planes respectively. A sharp reflection at 27° is indicative of the quartz silica sheets in MMT clay. The GO-MMT composite contains all the reflection of GO and MMT clay but with reduced intensity. The peak of GO at 10.5° is much diminished which may be due to exfoliation of GO in the hybrid nanocomposite. The XRD pattern of BR9@GO-MMT also shows a similar pattern but with further decrement in peak intensity.

The TGA curve of GO, MMT, GO-MMT and dye encapsulated GO-MMT is shown in figure S3. In the case of GO, the first weight loss occurs at around 100℃ due to the absorbed water molecules. The main mass loss occurs around 150-220 ℃, which can be attributed to the decomposition of labile oxygen functional groups such as carbonyl, epoxy and hydroxyl. The pure clay presented a considerable amount of mass loss at around 110 ℃ due to the loss of molecular water from its interlayer justifying its hydrophilic nature. The GO-clay composite exhibited lesser mass loss compared to the pristine GO and MMT sample by a considerable amount. A lesser amount of mass loss around 200 ℃ can be ascribed to the reduction of the labile oxygen functional group of GO in the GO-MMT composite. The dye-loaded GO-MMT composite showed weight loss at 100 ℃ due to the loss of absorbed water molecules. A considerable mass loss was observed in the range 260-450 ℃ which is an indication of the thermal degradation of the aromatic structure of the encapsulated dye molecule in the composite.

The SEM image indicating the surface morphology of GO, MMT, GO-MMT and BR9@GO-MMT are displayed in Fig. S4. SEM image of GO portrays

folded sheet-like wrinkled layered structure which is possibly due to aggregation of individual graphite sheets. The image of MMT clay was seen as a layered structure with an agglomeration of variable-sized particles. From the SEM image of the GO-MMT composite, it can be seen that it displays minor disorder with a combination of both MMT plate-like particles and GO sheets spread on the porous surface of the clay. This indicates that GO is not only intercalated in between the MMT layer but also spreads onto the external surface of clay. The dye intercalated nanohybrid show a similar image but exhibits more agglomeration of particles due to its adsorption on the surface of the nanocomposite. The EDX analysis of BR9@GO-MMT reveals the presence of the characteristic elements like Si, O, K, Mg, Ca, Al, C, N, Cl. The EDX elemental mapping in Fig. S5 also confirms the successful formation of dye intercalated GO-MMT composite.

BR9@GO-MMT as Fluorescent Sensor for DA

0.05 g of BR9@GO-MMT composite was dispersed in 10 mL acetonitrile and sonicated for 15 mins to get a fine dispersion. From the UV-Vis spectrum measurement (Fig. S6a), the excitation wavelength for the dispersed composite was fixed at 280 nm. The solution was taken in a quartz cuvette of path length 1 cm and irradiated with 280 nm of photons and the emission range was kept constant within the 280-600 nm range. The fluorescence peak for the sensor was observed at 343.4 nm with an intensity *ca.* 27. The fluorescence spectrum of BR9@GO-MMT in acetonitrile is shown in Fig. S6b, λ_{ex}=280 nm, λ_{max} = 343.4 nm.

50µL of different biomolecules such as AA, DA, UA, glucose, cholesterol, creatinine (10^{-3} M) and ions such as Na^+, K^+, Fe^{2+}, Ca^{2+} (10^{-3} M) were added one at a time into the cuvette containing the solution of BR9@GO-MMT and its fluorescent spectrum was recorded. The fluorescence intensity increased only in case of DA addition as shown in Fig. 1. Fig. 2 shows the gradual increment of fluorescence intensity of BR9@GO-MMT on addition of different concentrations of DA in PBS (*p*H = 7.39). The final enhancement of fluorescence peak intensity of BR9@GO-MMT is *ca.* 29 times the initial intensity upon the addition of 100 µL of DA. The inset of Fig. 2 implies that the plot of fluorescence intensity *vs.* the concentration of DA is linear with R^2 = 0.9943. The linear range was found to be

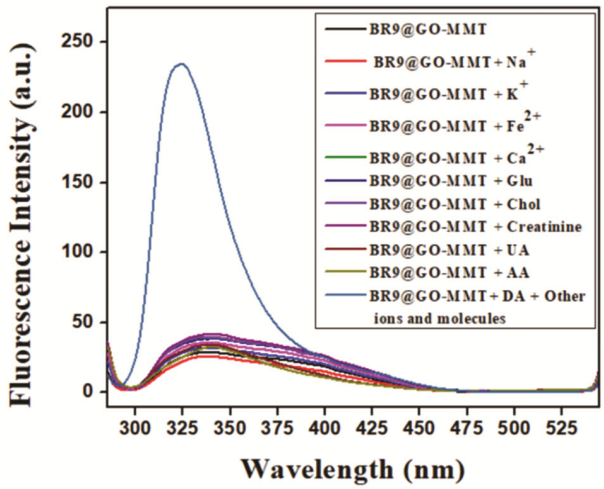

Fig. 1 — Effect of different biomolecules on Fluorescence Intensity of BR9@GO-MMT in acetonitrile.

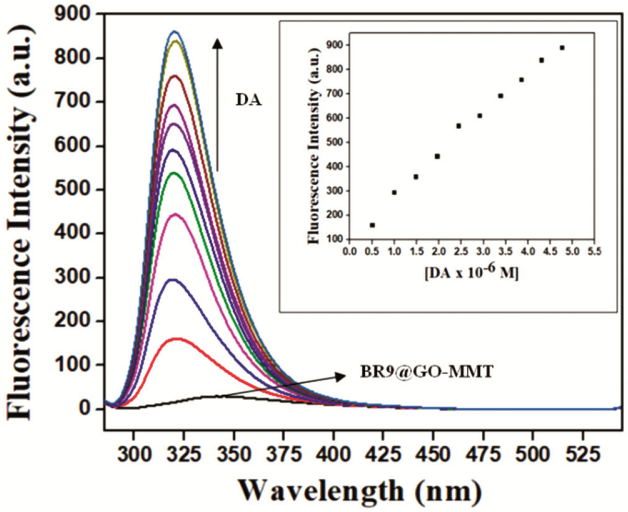

Fig. 2 — Fluorescence spectra of BR9@GO-MMT at different added concentrations of DA (0-100µL) in PBS (*p*H=7.39, λ_{ex}=280 nm, λ_{max}= 343.8 nm). The inset shows the plot of fluorescence intensity as a function of different concentration of DA.

0.5×10^{-6} M to 5×10^{-6} M. The fluorescent spectrum of BR9@GO-MMT towards its detection of DA was measured in presence of its two major biological interferential molecules *i.e.* AA and UA. It can be inferred from Fig. 3 that DA could enhance the fluorescence intensity of BR9@GO-MMT even in presence of AA and UA. The increment was found to be *ca.* 26 times upon the addition of 100 µL of DA in a medium containing both AA and UA. The linear range for the plot of fluorescence intensity *vs.* the concentration of DA was found to be 0.5×10^{-6} M to 5×10^{-6} M with R^2 = 0.9955 (Fig. 3, inset). The Limit of Detection (LOD) was calculated using the

formula[39]: 3S/K, where S = standard deviation, K= Slope obtained from the plot of fluorescence intensity *vs.* concentration of DA. It was found to be 6.57 nM and 5.05 nM in the absence and presence of AA and UA respectively.

UV-Visible spectral titrations were carried out for BR9@GO-MMT with DA in the absence and presence of interfering molecules, AA and UA. Fig. 4 shows the UV-Vis spectral data of BR9@GO-MMT in acetonitrile at different added concentrations of DA. It can be seen that the hump at 290 nm gradually increases on the addition of DA. The same result can be seen in the case of UV-Vis spectral titration of DA in presence of AA and UA (Fig. 5). Furthermore, the plot of absorbance *vs*. DA concentration is in the linear range and similar to that procured from fluorescence data.

The elevation in fluorescence intensity of BR9@GO-MMT on interaction with DA was found to be reversible. The reversibility of the sensor was checked with the help of chelator Na_2EDTA (10^{-2} M). When $EDTA^{2-}$ was added gradually to the solution of BR9@GO-MMT containing one equivalent of DA, its fluorescence intensity was found to decrease regularly (Fig. 6). This gradual decrease observed in the

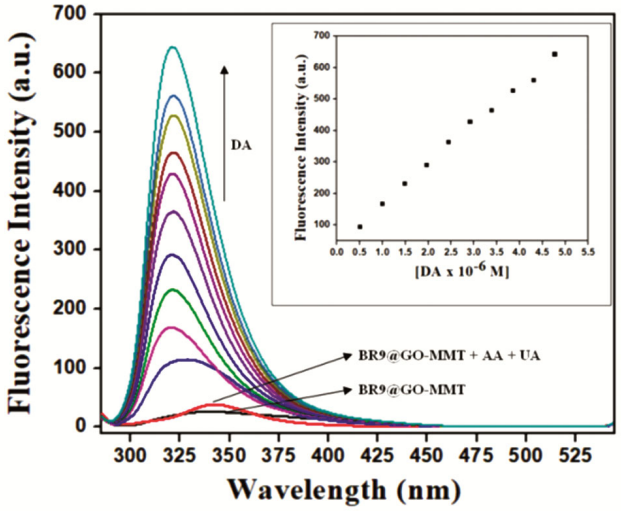

Fig. 3 — Fluorescence spectra of BR9@GO-MMT at different added concentrations of DA (0-100µL) in presence of AA and UA (*p*H=7.39, λ_{ex}=280 nm, λ_{max}= 342.6 nm). The inset shows the plot of fluorescence intensity as a function of different concentration of DA in presence of AA and UA.

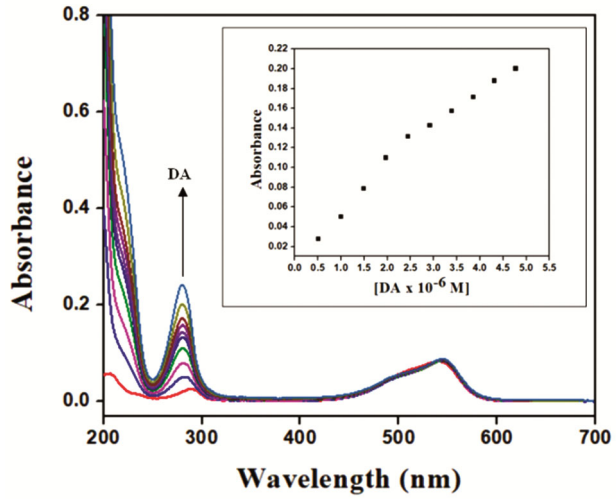

Fig. 4 — UV-Vis spectra of BR9@GO-MMT with different added concentrations of DA (0-100µL). The inset shows the plot of absorbance as a function of DA concentration.

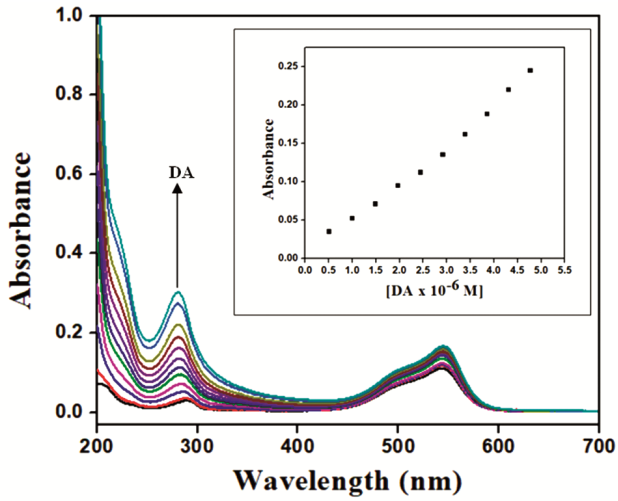

Fig. 5 — UV-Vis spectra of BR9@GO-MMT with different added concentrations of DA (0-100µL) in presence of AA and UA. The inset shows the plot of absorbance as a function of DA concentration.

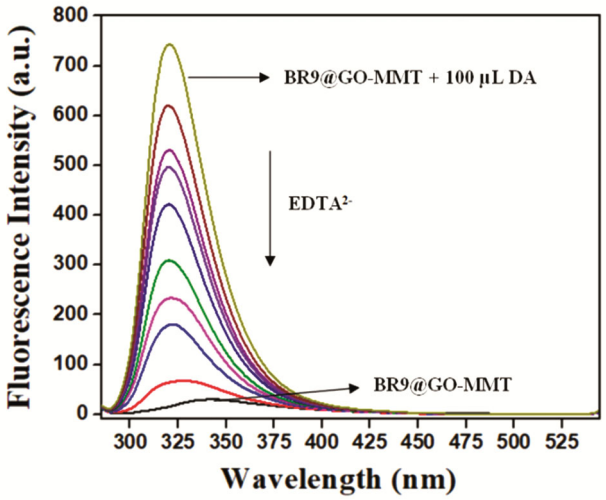

Fig. 6 — Fluorescence spectra of BR9@GO-MMT:DA at different added concentration of $EDTA^{2-}$

fluorescence intensity is due to the formation of a complex between DA and $EDTA^{2-}$ leaving the sensor BR9@GO-MMT free.

Biological Application

Detection of DA in Bovine Serum Albumin (BSA)

The ability of BR9@GO-MMT to detect DA in the BSA medium was carried out successfully. For this purpose, 5 mL of BR9@GO-MMT in PBS (*p*H = 7.39) was spiked with 2 mL of BSA. The spiked BR9@GO-MMT solution was then titrated against DA. Fig. 7 shows the gradual enhancement of fluorescence intensity of BR9@GO-MMT by *ca.* 20 times on gradual addition of DA. The plot of fluorescence intensity *vs.* DA in BSA medium was found to be linear with a linear range of 0.5×10^{-6} M to 5×10^{-6} M. The LOD in the BSA medium was calculated to be 2.87 nM.

Electrochemical sensing of DA in presence of AA and UA by BR9@GO-MMT/GC

The sensing ability of BR9@GO-MMT towards its detection of DA in presence of AA and UA were conducted by cyclic voltammetry (CV) technique. A three-electrode cell system consisting of modified glassy carbon (GC) electrode as the working electrode, Ag-AgCl as the reference electrode and Pt wire as the auxiliary electrode was used to conduct the electrochemical experiments.

Figure S7 depicted the CV curves obtained for 2 mM potassium ferrocyanide at both bare GC electrode (black line) and modified GC electrode (red line) in presence of 1M KCl as supporting electrolyte at scan rate 50 mV/s. The BR9@GO-MMT/GC electrode showed relatively improved peak current signals in comparison to the bare GC electrode. Furthermore, the potential difference (ΔE) for the bare GC electrode and the modified GC electrode was found to be 0.8160 V and 0.2446 V respectively. This result confirms the improved electrocatalytic activity of the GC electrode due to its surface modification. The total active surface area of the modified electrode was calculated using the Randles-Sevick's equation[40]:

$$Ip = (2.69\times10^{5})\, n^{3/2}\, A\, D^{1/2}\, Cv^{1/2}$$

The electroactive surface area for the bare GC electrode and BR9@GO-MMT/GC electrode was calculated to be 0.1456 cm^2 and 0.1886 cm^2 respectively. The chronocoulometry plot of BR9@GO-MMT/GC electrode showed an elevated signal as compared to the bare GC electrode (Fig. S7). This outcome confirms the amplification of the electron transfer rate of the BR9@GO-MMT/GC electrode due to its enhanced conductivity and larger surface area.

The CV response of the BR9@GO-MMT/GC electrode in PBS buffer (*p*H=7.39) from a potential range of +1.400 V to -1.000 V in presence of 1.0 mM AA (Fig. S8). The irreversible oxidation peak of AA appears at 0.352 V on the electrode. The peak signal also increases on increasing the concentration of AA with a good linear concentration range (R^2 = 0.9978). The CV for detection of 0.1 mM UA by the BR9@GO-MMT/GC electrode shows an irreversible oxidation peak at 0.670 V (Fig. S9). The CV curve of the BR9@GO-MMT/GC electrode shows a reversible response in presence of 0.01 mM DA, with the cathodic peak appearing at 0.192 V and the anodic peak appearing at 0.4552 V respectively (Fig. S10). Furthermore, the current signals of UA and DA were all gradually increased with rising levels of the analyte and also achieved a good linear relationship (Insets, Fig. S9 and Fig. S10). The coefficient of determination *i.e.* R^2 for UA and DA detection was found to be 0.9888 and 0.9913 respectively. The LOD (limit of detection) was calculated using the equations[39]: 3S/K, where S = standard deviation, K = slope of the current *vs.* concentration graph. The LOD for AA, UA and DA were obtained as 1.165 nM, 0.875 nM and 3.043 nM respectively.

In order to establish that BR9@GO-MMT/GC electrode could simultaneously detect these three small

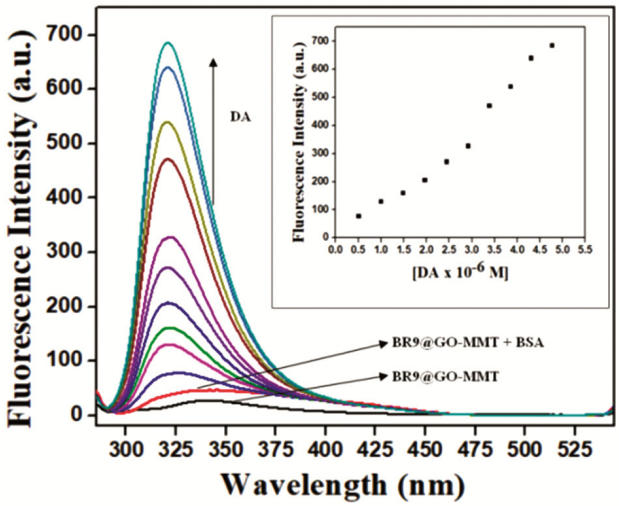

Fig. 7 — Fluorescence spectra of BR9@GO-MMT at different added concentrations of DA in BSA medium (PBS, *p*H 7.39). The inset shows the plot of fluorescence intensity *vs.* DA concentration.

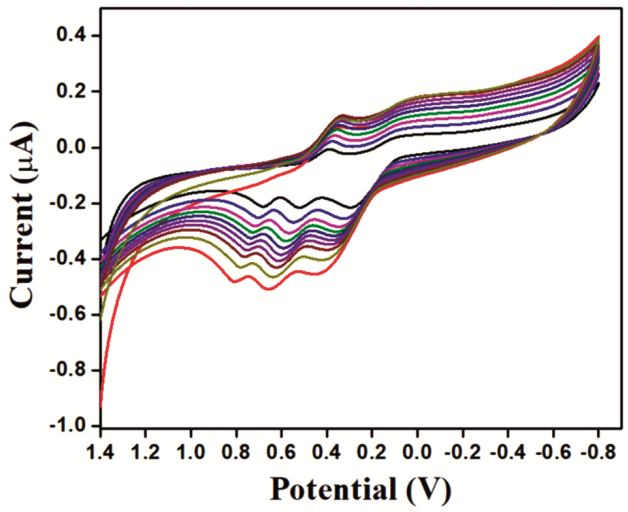

Fig. 8 — CV response of BR9@GO-MMT/GC in PBS (*p*H = 7.39) at simultaneous addition of 1mM AA, 0.1 mM UA and 0.01 mM DA. (RE: Ag-AgCl, SE: 1M KCl, scan rate: 50 mV/s)

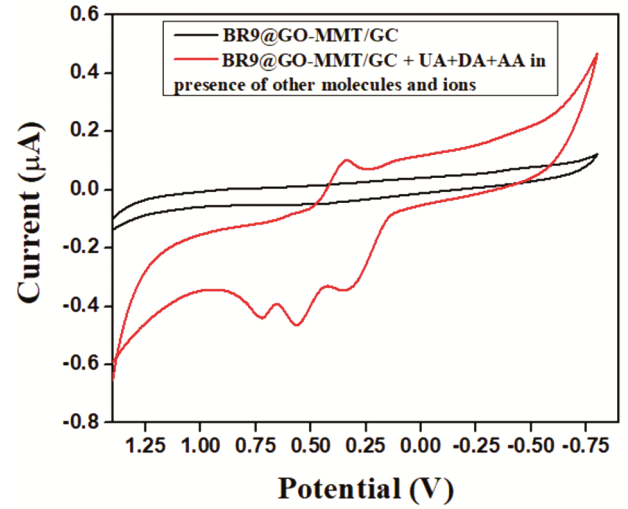

Fig. 9 — CV response of 1 mM AA, 0.1 mM UA and 0.01 mM DA in presence of interfering ions and molecules at BR9@GO-MMT/GC in PBS (*p*H = 7.39). (RE: Ag-AgCl, SE: 1M KCl, scan rate: 50 mV/s)

biological compounds, the CV was recorded in a mixture containing 1 mM AA, 0.1 mM UA and 0.01 mM DA in PBS. As Fig. 8) shows, the modified electrode could produce three well-defined separate peaks corresponding to AA, DA and UA respectively. The oxidation peaks for AA, DA and UA appear at +0.389 V, +0.608 V and +0.754 V respectively. The peak current signals increase with the gradual addition of the mixture and also the peak potential shifts towards the left side. The peak separation is high, which is an indication that the modified electrode could fasten the electron transfer rate of AA, DA and UA due to its adsorption on the electrode surface. This outcome suggests that BR9@GO-MMT/GC could generate good separation capacity towards AA, DA and UA in either selective or simultaneous detection.

Influence of other substances in the simultaneous voltammetric detection of AA, DA and UA

To evaluate the influence of biologically significant ions and molecules that co-exist with AA, DA and UA, the CV for the mixture was recorded in presence of a 100-fold concentration of Na^+, K^+, Ca^{2+}, Fe^{2+}, glucose and cholesterol. Fig. 9 shows that the presence of these interfering ions and molecules did not produce any significant changes in the current signals of AA, DA and UA. This result depicts higher current sensitivity and helps in a precise detection of AA, DA and UA at BR9@GO-MMT/GC electrode. The modified GC electrode has also been employed to detect DA in a mixture containing AA and UA in BSA medium with a linear range and LOD similar to that in PBS (*p*H = 7.39).

In conclusion, The dye Basic Red 9 has been successfully encapsulated in Graphene oxide-montmorillonite composite. This encapsulated GO-MMT sensor can detect neurotransmitter dopamine by fluorescence "on" mode in phosphate buffer solution at *p*H 7.39 as well as in the bovine serum albumin in the presence of ascorbic acid, uric acid, glucose, cholesterol and metal ions of Na^+, K^+, Ca^{2+}, Fe^{2+}. The linear range of detection is 0.5×10^{-5} M to 5.0×10^{-5} M with limits of detection in nanomolar range. Glassy carbon electrode modified with the dye encapsulated GO-MMT sensor affects oxidation peak to peak separation for DA-UA at +0.147 V and that of DA-AA at +0.235 V. The linear range of detection for dopamine by voltammetry is 5×10^{-5} M to 50.0×10^{-5} M with limits of detection in nanomolar range in presence of interfering ions and molecules in phosphate buffer solution at *p*H 7.39 as well as in bovine serum albumin.

Supplementary Information

Supplementary information is available in the website http://nopr.niscpr.res.in/handle/123456789/58776.

Acknowledgement

The authors thank DST, New Delhi for FIST to the department and for MRP (EMR/2016/001745) to DKD.

References

1 Jia N Q, Wang Z Y, Yang G F, Shen H B & Zhu L Z, *Electrochem Commun*, 9 (2007) 233.
2 Wightman R M, May L J & Michael A C, *Anal Chem*, 60 (1988) 769.
3 Wightman R M & Robinson D L, *J Neuro chem*, 82 (2002) 721.
4 Cao X, Luo L, Ding Y, Zou X & Bian R, *Sens Actuators B Chem,* 2 (2008) 941.
5 Harris W H & Petten G R V, *Am J Obstet Gynecol*, 130 (1978) 211.
6 Zhang X, Chen X, Kai S, Wang H Y, Yang J, Wu F G & Chen Z, *Anal Chem*, 87 (2015) 3360.
7 Oak J N, Oldenhof J & Tol H H V, *Eur J Pharmacol*, 405 (2000) 303.
8 Adekunle A S, Agboola B O, Pillay J & Ozoemena K I, *Sens Actuator B Chem*, 148 (2010) 93.
9 Zhang L, Teshima N, Hasebe T, Kurihra M & Kawashima T, *Talanta*, 50 (1999) 677.
10 Liu J M, Cui M L, Jiang S L, Wang X X, Lin L P, Jiao L, Zhang L H & Zheng Z Y, *Anal Methods*, 5 (2013) 3942.
11 Kim Y, Bong S, Kang Y, Yang Y, Mahajan R K, Kim J S & Kim H, *Biosens Bioelectron*, 25 (2010) 2366.
12 Wang A, Feng J, Dong W, Lu Y, Li Z & Riekkola M L, *J Chromatogr A*, 1217 (2010) 5130.
13 Su H, Sun B, Chen L, Xu Z & Ai S, *Anal Methods*, 4 (2012) 3981.
14 Mu Q, Xu H, Li Y, Ma S & Zhong X, *Analyst*, 139 (2014) 93.
15 Li N, Gao J, Liu B, Yu Y, Cui H, Mao L & Lin Y, *Anal Chim Acta*, 645 (2009) 48.
16 Gonzalez R R, Fernandez R F, Vidal J L M, Frenich A G & Perez M L G, *J Neurosci Methods*, 198 (2011) 187.
17 Meng S, Liu Y, Wang L, Ji X, Chen Y, Zheng T, Yu J & Feng H, *Front Bioeng Biotech*, 9 (2021) 726071.
18 Salimi A, Mam-Khezri H & Hallaj R, *Talanta*, 70 (2006) 823.
19 Shashikumara J K & Kumara Swamy B E, *Sensors Intl*, 1 (2020) 100008.
20 Kalita S & Das D K, *J Fluoresc*, 32 (2021) 235.
21 Geim A K & Novoselov K S, *Nat Mater,* 6 (2007) 183.
22 Zhu Y, Murali S, Cai W, Li X, Suk J W & Potts J R, *Adv Mater*, 22 (2010) 3906.
23 Yang S T, Chen S, Chang Y, Cao A, Liu Y & Wang H, *J Colloid Interface Sci*, 359 (2011) 24.
24 Wang B, Zhang F, He S, Huang F & Peng Z, *Asian J Chem*, 26 (2014) 4901.
25 Björk J, Hanke F, Palma C A, Samori P, Cecchini M & Persson M, *J Phys Chem Lett*, 1 (2010) 3407.
26 Neelaveni M, Santhana Krishnan P, Ramya R, Sonia Theres G & Shanthi K, *Adv Powder Technol*, 3 (2019) 569.
27 Zhao J, Liu F, Wang Z, Cao X & Xing B, *Environ Sci Technol*, 49 (2015) 2849.
28 Yang S, Ren X, Zhao G, Shi W, Montavon G, Grambow B & Wang X, *Geochim Cosmochim Acta*, 166 (2015) 129.
29 Songyang Y, Yang X, Xie S, Hao H & Song J, *Food Chem*, 173 (2015) 640.
30 Shetti N P, Nayak D S, Kuchinad G S & Naik R R, *Electrochim Acta*, 269 (2018) 204.
31 Zhao C, Qin H, Gong F, Feng M, Zhang S &Yang M, *Polym Degrad Stabil*, 87 (2015) 183.
32 Tandel R D, Pawar S K & Seetharamappa J, *J Electrochem Soc*, 163 (2016) H705.
33 Ding S N, Zheng C L, Wan N & Cosnier S, *Monatsh Chem*, 145 (2014)1389.
34 Li M, Zhu J E, Zhang L, Chen X, Zhang H, Zhang H, Zhang F, Xu S & Evans D G, *Nanoscale*, **3** (2011) 4240.
35 Sareen D, Kaur P & Singh K, *Coord Chem Rev*, 265 (2014) 125.
36 Erdem A, Kerman K, Meric B, Akarca U S & Ozsoz M, *Anal Chim Acta*, 422 (2000) 139.
37 Su S, Hao Q, Yan Z, Dong R, Yang R, Zhu D, Chao J, Zhou Y & Wang L, *Microchim Acta*, 186 (2019) 607.
38 Rajbongshi J, Das D K & Mazumdar S, *Electrochim Acta*, 55 (2010) 4174.
39 Lai X, Wang R, Li J, Qiu G & Liu J B, *RSC Adv*, 9 (2019) 22053.
40 Kuskur C M, Kumara Swamy B E, Jayadevappa H & Shivakumar K, *Anal Chem Insights*, 3 (2017) 1.